# Quantitative Assessment of In Vivo Breast Masses Using Ultrasound Attenuation and Backscatter

Ultrasonic Imaging
35(2) 146–161

DOI: 10.1177/0161734613480281
ultrasonicimaging.sagepub.com

**Kibo Nam[1], James A. Zagzebski[1], and Timothy J. Hall[1]**

## Abstract

Clinical analysis of breast ultrasound imaging is done qualitatively, facilitated with the ultrasound breast imaging–reporting and data system (US BI-RADS) lexicon, which helps to standardize imaging assessments. Two descriptors in that lexicon, "posterior acoustic features" and the "echo pattern" within a mass, are directly related to quantitative ultrasound (QUS) parameters, namely, ultrasound attenuation and the average backscatter coefficient (BSC). The purpose of this study was to quantify ultrasound attenuation and backscatter in breast masses and to investigate these QUS properties as potential differential diagnostic markers. Radio frequency (RF) echo signals were from patients with breast masses during a special ultrasound imaging session prior to core biopsy. Data were also obtained from a well characterized phantom using identical system settings. Masses include 14 fibroadenomas and 10 carcinomas. Attenuation for the acoustic path lying proximal to the tumor was estimated offline using a least squares method with constraints. BSCs were estimated using a reference phantom method (RPM). The attenuation coefficient within each mass was assessed using both the RPM and a hybrid method, and effective scatterer diameters (ESDs) were estimated using a Gaussian form factor model. Attenuation estimates obtained with the RPM were consistent with estimates done using the hybrid method in all cases except for two masses. The mean slope of the attenuation coefficient versus frequency for carcinomas was 20% greater than the mean slope value for the fibroadenomas. The product of the attenuation coefficient and anteroposterior dimension of the mass was computed to estimate the total attenuation for each mass. That value correlated well with the BI-RADS assessment of "posterior acoustic features" judged qualitatively from gray scale images. Nearly all masses were described as "hypoechoic," so no strong statements could be made about the correlation of echo pattern findings in BI-RADS with the averaged BSC values. However, most carcinomas exhibited lower values for the frequency-average BSC than fibroadenomas. The mean ESD alone did not differentiate the mass type, but fibroadenomas had greater variability in ESDs within the ROI than that found for invasive ductal carcinomas. This study demonstrates the potential to use attenuation and QUS parameters associated with the BSC as quantitative descriptors.

[1]Department of Medical Physics, University of Wisconsin–Madison, WI, USA

**Corresponding Author:**
Timothy J. Hall, Department of Medical Physics, University of Wisconsin–Madison, 1111 Highland Ave., Madison, WI 53705, USA.
Email: tjhall@wisc.edu

**Keywords**

BI-RADS, breast cancer, attenuation, backscatter, ultrasound, quantitative ultrasound, fibroadenoma, carcinoma, biomarker

## Introduction

Ultrasound is a valuable tool to use in conjunction with x-ray mammography for diagnosing breast masses. A common use of ultrasound in breast imaging is to distinguish between cystic and solid masses. However, ultrasound can also assist in differentiating among different solid masses. Clinically, the modality is most useful in assessing very dense breasts because the sensitivity of mammography for dense breast conditions is low (35%-48%).[1]

Considerable progress has been made to establish ultrasound criteria for differentiating benign from malignant breast tumors.[2-6] Various sonographic features, including a lesion's margin, its shape, and its internal echo texture are evaluated.[3,7,8] Malignant masses are often characterized by poorly defined margins on ultrasound B-mode images, irregular and sometimes spiculated boundaries, microlobulations, hypoechogenicity, and shadowing. They sometimes are associated with duct extension and tissue architectural distortion. Benign masses, however, more often have well-defined and circumscribed boundaries, and round or oval shapes with gentle bi- or trilobulations.[9] Several studies[10,11] evaluated the interobserver variability in judging these features. Rahbar et al.[11] agreed that although such features help differentiate benign from malignant breast masses, there was a need to investigate their practice and interpreter variability. Arger et al.[10] found that the interpretations made by four different readers were comparable when standardized descriptors of breast masses were applied.

In 2003, the American College of Radiology (ACR) developed the first edition of a lexicon, the Ultrasound Breast Imaging–Reporting and Data System (US BI-RADS), to standardize the interpretation and reporting of breast masses in ultrasound.[12] Hong et al.[13] demonstrated that the US BI-RADS descriptors involving lesion margin, shape, orientation, lesion boundary, and internal echo pattern, as well as acoustic features posterior to a mass, can be used in differentiating benign from malignant conditions. After applying US BI-RADS criteria, they reported a positive predictive value (PPV) for malignancy of 62% to 86%.[13] The PPVs reported by Hong et al. were comparable with PPV values obtained (68%-81%) when applying the BI-RADS descriptors for x-ray mammography as reported by Liberman et al.[14]

Conventional B-mode ultrasound imaging itself is a qualitative modality because image brightness and other features of displayed echo signals depend on operator settings and on system- and tissue-dependent factors. The subjective interpretation and only moderate specificity result in most solid masses viewed on ultrasound also undergoing a core biopsy to provide a definitive diagnosis. This in turn leads to a high rate of biopsies of benign tumors, resulting in increased stress and burden to patients and high costs to the health care system.[9]

Quantitative ultrasound (QUS) is being studied as a means of aiding in this diagnosis. QUS methods extract estimates of attenuation and backscatter on absolute scales, as well as other features that depend on acoustic wave-tissue interactions. QUS has shown potential for detecting diffuse disease and for diagnosing focal lesions in a number of clinical tasks. For example, estimates of ultrasound attenuation from backscattered echo signals were used to differentiate fatty liver from normal liver.[15,16] Other researchers have demonstrated that ultrasound attenuation has diagnostic value in the trabecular bone,[17] the cortical bone,[18] and the breast.[19,20] In addition, spectral analysis of backscattered echo signals has been used successfully to differentiate benign from malignant masses in the eyes[21] and in lymph nodes,[22,23] and to outline high-risk regions to guide prostate biopsies.[24] A "scatterer size" descriptor was successfully applied to estimate glomerular and arteriole sizes in kidneys.[25] Also, preliminary data have been obtained to evaluate

the role of QUS in areas such as identifying malignant thyroid nodules[26] and liver masses.[27] Finally, estimation of the effective scatterer diameter (ESD) differentiated rat mammary fibroadenomas from 4T1 mouse carcinomas.[28]

The focus of this study is in quantifying attenuation and backscatter properties of breast masses and comparing results with related features reported clinically when applying US BI-RADS descriptors. Within US BI-RADS, echo patterns of breast masses are categorized as anechoic, hypoechoic, isoechoic, hyperechoic, or complex. Similarly, posterior acoustic features are described as none, enhancement, shadowing, and combined. Although these descriptors are closely related to the backscatter and the attenuation properties of breast masses, current clinical practice evaluates these features qualitatively and subjectively. This work is the next step in assessing these acoustic features quantitatively using local attenuation values and backscatter coefficients (BSCs; beyond the work of D'Astous and Foster[29]) and extends that work by comparing the quantitative estimates to the subjectively assessed BI-RADS descriptors. This study also investigates acoustic attenuation, averaged BSCs (ABSCs), and ESDs as QUS parameters for differentiating benign from malignant breast masses.

## Method

### *Data Collection*

Human subject protocols were University of Wisconsin Health Sciences Institutional Review Board approved and Health Insurance Portability and Accountability Act compliant. Fifty participants who were scheduled for an ultrasound-guided breast core biopsy of a suspicious mass were recruited. Participants were scanned with a Siemens S2000 (Siemens Medical Solutions USA, Inc., Malvern, Pennsylvania) using an 18L6 linear array transducer operated at a center frequency of 15 MHz. Using the Axius Direct ultrasound research interface (URI),[30] we obtained radio frequency (RF) echo data from longitudinal and transverse planes of the mass and surrounding tissues.

Reference phantom data were also obtained immediately after scanning the breast using the same transducer and equipment settings. The acoustic properties of the reference phantom had been estimated previously using a narrow-band substitution technique[31] applied to test samples manufactured at the same time as the reference phantom. The sound speed was 1492 m/s, measured at 2.5 MHz. Attenuation coefficients in the reference phantom, determined at frequencies from 2 to 10 MHz were fit to a linear function of frequency, yielding $\alpha(f)$ $(\mathrm{dB \cdot cm^{-1}}) = 0.54f$, where $f$ is the frequency in MHz. The scanning window of the reference phantom was a 25-μm-thick Saran™ film (Dow Chemical, Midland, Michigan). The BSCs were measured using a broadband reference reflector method with focused single element transducers.[32]

For this report, we restricted the analysis to masses diagnosed by core biopsy to be either fibroadenomas or carcinomas, and whose size was larger than 7 mm axially. This lesion size restriction was imposed to reduce bias and variance in parameter estimates[33] and resulted in retaining 17 of the total of 54 data sets. This group included 9 fibroadenomas, 5 invasive ductal carcinomas, and 1 each of invasive lobular carcinoma, intracystic papillary carcinoma, and adenocarcinoma.

We also included in this analysis data from seven patients scanned using an earlier protocol designed to evaluate breast elasticity imaging,[34] where RF echo data had also been acquired. These patients were scanned using a Siemens Antares (Siemens Medical Solutions USA, Inc., Malvern, Pennsylvania) equipped with a VFX13-5 linear array transducer operated at a center frequency of 10 MHz. RF echo data were recorded while the sonographer applied small deformations using the transducer, with an interframe strain of less than 1%. Each frame consisted of either 256 or 312 acoustic scan lines. Among the masses present in these seven patients, there

were five fibroadenomas, one invasive ductal carcinoma, and one invasive lobular carcinoma. As in the previous data set, echo signals also were recorded from a reference phantom using the same transducer and system settings. In this case, the reference phantom consisted of an emulsion containing 70% safflower oil,[35] covered with a plastic-coated aluminum foil (Gammex Inc., Middleton, Wisconsin). Properties of this reference phantom[31] were a speed of sound of 1492 m/s and an attenuation coefficient versus frequency slope of 0.54 dB·cm$^{-1}$MHz$^{-1}$. Similar to the reference described above, BSCs were measured using a broadband reference reflector method.[32]

## Attenuation Coefficient Estimations

Two methods were used to estimate the local attenuation within the masses: A reference phantom method (RPM)[36] and a "hybrid method."[37] Both methods are based on computations of the echo signal power spectral density from a region, and both apply data from the reference phantom to account for system-dependent factors on the echo data.[38] For a uniform region in the tissue, referred to as a "parameter estimation region" (PER), the ratio of the echo signal power spectrum at depth $z$, $S_{\text{sam}}(f, z)$ to $S_{\text{ref}}(f, z)$, the echo signal power spectrum from the same depth in the reference medium, can be written as,[36]

$$\frac{S_{\text{sam}}(f,z)}{S_{\text{ref}}(f,z)} = \frac{B_{\text{sam}}(f)\exp\{-4\alpha_{\text{sam}}(f)z\}}{B_{\text{ref}}(f)\exp\{-4\alpha_{\text{ref}}(f)z\}}, \tag{1}$$

where $B(f)$s are BSCs at frequency $f$, the $\alpha(f)$ values represent attenuation coefficients, and the subscripts *sam* and *ref* designate the sample and the reference phantom, respectively. Assuming $B_{\text{sam}}(f)$ is constant over the PER, the attenuation coefficient within that region may be computed using

$$\alpha_{\text{sam}}(f) = -\frac{\ln\left(\frac{S_{\text{sam}}(f,z)}{S_{\text{ref}}(f,z)}\right)\Big|_{z2} - \ln\left(\frac{S_{\text{sam}}(f,z)}{S_{\text{ref}}(f,z)}\right)\Big|_{z1}}{4(z_2 - z_1)} + \alpha_{\text{ref}}(f), \tag{2}$$

where $z_1$ and $z_2$ are different depths within the PER in the mass, with $z_2 > z_1$.

A "hybrid" technique, shown to be less prone to artifacts from backscatter variations than the RPM,[36] was also applied. It evaluates changes in the center frequency of the sample-to-reference power spectra ratio with depth after applying a Gaussian frequency filter to this ratio. Kim and Varghese[37] assumed a linear frequency dependence of the attenuation and modeled the BSC $B(f)$ with a simple power law. Then, the relationship between $\alpha_0$, the attenuation coefficient in dB·cm$^{-1}$MHz$^{-1}$, and the slope of the downshifted center frequency versus depth, $df_c(z)/dz$, is given by[37]

$$\alpha_{0,\text{sam}} = -\frac{8.686}{4\sigma^2}\cdot\frac{df_c(z)}{dz} + \alpha_{0,\text{ref}}, \tag{3}$$

where $\sigma^2$ is the bandwidth of the transmit pulse.

During breast scanning, the sonographer marked the limits of the mass that was to be biopsied, placing fiducial marks near the tumor margins as viewed on B-mode, color flow, and elasticity images. These served as guides during offline analysis. She also measured the dimensions in the acoustic scan line direction using digital calipers. For either attenuation estimation technique, we defined a PER within the mass that was judged to be homogeneous, avoiding

distinct boundary echoes, specular reflectors, and specular highlights. The power spectrum analysis window size was 3 mm (axially, eight pulse lengths) by 3 mm (laterally, six uncorrelated acoustic scan lines). Analysis windows overlapped axially and laterally by 90% over the PER, and power spectra were calculated using Welch's periodogram[39] with a 2-mm Hann window and the chirp z-transform (CZT).[40] The analysis bandwidth was chosen independently for each mass to select a frequency range where the signal was at least 10 dB above the noise floor. In all cases, the lower limit of the bandwidth was between 3 MHz and 4 MHz, whereas the upper limit ranged from 8 MHz to 13 MHz for different patients, depending on the depth of the PER. Ratios of the power spectra from the mass to those from the reference were calculated over the PER, and the slope of the attenuation coefficient versus frequency was determined using the entire axial length of the PER, applying either (2) or (3). When multiple PERs could be identified within a mass, attenuation coefficient estimates for the different PERs were averaged to obtain a final result using each method.

### *BI-RADS Descriptor "Posterior Acoustic Features"*

The BI-RADS descriptor "posterior acoustic features" mainly expresses the degree of attenuation within a mass. To investigate further, the region distal to each mass was assessed on B-mode images by one radiologist and two physicists who are familiar with the BI-RADS criteria and how ultrasound–tissue interactions contribute to B-mode image features. The physicists also reviewed BI-RADS sonographic criteria through discussions with breast radiologists, including reviewing images containing different examples of features. Each observer conducted the assessment independently by subjectively comparing the B-mode image brightness distal to the mass with the brightness of the adjacent tissue (at the same depth). Due to interobserver variability, the final assessment of the posterior acoustic feature was determined based on the majority opinion from the three observers. When there was no majority opinion, the posterior acoustic feature was rated as "competing interpretation."

### *BSC Determinations*

Echogenicities of masses were quantified by computing the BSC, applying the reference phantom technique as in (1).[36] For BSC estimation, it is necessary to compute the total ultrasound attenuation from the skin surface to the PER.

We define an "effective attenuation coefficient," $\alpha_{\text{eff}}(f)$, to represent attenuation for the entire tissue path above each BSC PER. A least squares method (LSM) has been shown to provide accurate assessments of attenuation when this path is inhomogeneous, such as many cases in the breast scanned here.[38] The LSM approximates the total attenuation in (1) as having a linear frequency dependence so the total attenuation losses are modeled as $\exp(-\alpha_{\text{eff}} f z)$, where $z$ is the depth to the midpoint of the backscatter PER. Similarly, the BSC $B(f)$ within the PER is modeled using a power law, $B(f) = b f^n$. From (1), the ratio of the echo signal power spectrum from the sample to that from the reference phantom at the same depth can be expressed as follows:

$$\frac{S_{\text{sam}}(f,z)}{S_{\text{ref}}(f,z)} = \frac{b_{\text{sam}} f^{n_{\text{sam}}}}{b_{\text{ref}} f^{n_{\text{ref}}}} \exp\left\{-4\left(\alpha_{\text{eff,sam}} - \alpha_{\text{eff,ref}}\right) f \cdot z\right\}. \tag{4}$$

To solve for the $b_{\text{sam}}(f)$, $n_{\text{sam}}$, and $\alpha_{\text{eff,sam}}$ in (4), a least squares fitting process is applied over the band of frequencies contained in the backscattered signal.[38] To keep the solutions within realistic ranges, the following constraints were imparted during the LSM:

$$10^{-7} \le b_{\text{sam}} \le 10^{-1},\ 0 \le n_{\text{sam}} \le 5,\ 0.2 \le \alpha_{\text{eff,sam}} \left(\text{dB} \cdot \text{cm}^{-1} \cdot \text{MHz}^{-1}\right) \le 2). \quad (5)$$

The total attenuation over the path above a backscatter PER was accounted for from the estimated effective attenuation coefficient at the depth of the PER. Then, the estimated BSCs for PERs within the mass were averaged to obtain the final result.

One use of these data was to compare with subjective descriptors of the echo level according to the BI-RADS lexicon. To do this, the $B(f)$ values computed for the mass were averaged[41,42] over the central frequency range of the echo signal power spectrum (from ~5 to 8 MHz for our cases). The echo pattern of each mass was subjectively evaluated on B-mode images by comparing the echo level within the mass with the echo level of fat surrounding the mass. Just as with the attenuation and posterior feature data, the final determination of the echo pattern was based on a majority opinion. When there was no majority opinion, the echo pattern of the mass was rated as "competing interpretation." The echo pattern of each mass was also compared with its "ABSC" results.

### ESD Estimation

The ESD was estimated from the BSCs over the central frequency range (5-8 MHz) using a Gaussian form factor, a model used by many researchers for describing scattering from biological tissues.[43-47] In the case of a Gaussian form factor model, the ESD can be estimated by a minimax approach[48] and is given as follows:

$$\hat{a}^2 = -\frac{d_1^{\,2} c^2}{80} \frac{\sum_{f_i=f_{\min}}^{f_{\max}} \left( y(f_i) f_i^2 - \overline{y(f)}\,\overline{f^2} \right)}{\sum_{f_i=f_{\min}}^{f_{\max}} \left( f_i^2 - \overline{f^2} \right)^2}, \quad (6)$$

where $f$ is the frequency, $y(f) = 10\ln(B(f)/f^4)$, $d_1 = (12\sqrt{2\pi})^{1/3}$, and $c$ is the speed of sound. $B(f)$ is the BSC at frequency $f$. Also, $\overline{y(f)} = 1/N \sum_{f_i=f_{\min}}^{f_{\max}} \overline{y(f_i)}$, $\overline{f^2} = 1/N \sum_{f_i=f_{\min}}^{f_{\max}} f_i^2$, where $N$ is the number of discrete frequencies between $f_{\min}$ and $f_{\max}$. The form factor approach uses a model to describe frequency-dependent deviations in the BSC from that from Rayleigh (point-like) scatterers, which have an $f^4$ frequency dependence. A Gaussian model for the form factor is a common and convenient choice when there is little known about the sources of scattering in the tissue being studied.

## Results

### Comparison of Attenuation Coefficient Estimates

The estimated slope of the attenuation coefficient versus frequency for each mass is listed in Table 1. The patient number was assigned here to group similar pathology results so that the attenuation variation among different mass types can be easily noted. Inspection of the data in columns 3 and 4 reveals that the RPM and the hybrid method provided comparable results. That is, the difference in the estimates using the hybrid method and the RPM ranged from 0.7% to 43.9%, and the mean difference was 12.0%. The results using the two methods were consistent, with the exception of two of the fibroadenoma cases, Patients 12 and 14.

To assess possible attenuation changes among different types of masses, the attenuation coefficient versus frequency slope estimates from the 14 fibroadenomas were averaged, as were those for the 10 carcinomas. The mean values for both tumor types are shown in Figure 1. The

**Table 1**. Estimated Slope of the Attenuation Coefficient versus Frequency from 24 Masses Using the RPM and Hybrid Method.

| Patient Number | Biopsy Result | RPM Result ($dB \cdot cm^{-1}MHz^{-1}$) | Hybrid Result ($dB \cdot cm^{-1}MHz^{-1}$) | % Difference in Estimates |
|---|---|---|---|---|
| 1 | Fibroadenoma | 1.06 | 0.90 | −15.1 |
| 2 | Fibroadenoma | 0.44 | 0.47 | +6.8 |
| 3 | Fibroadenoma | 0.97 | 1.12 | +17.5 |
| 4 | Fibroadenoma | 1.29 | 1.30 | +0.8 |
| 5 | Fibroadenoma | 1.12 | 1.05 | −6.2 |
| 6 | Fibroadenoma | 1.02 | 1.17 | +14.7 |
| 7 | Fibroadenoma | 1.01 | 0.91 | −9.9 |
| 8 | Fibroadenoma | 1.63 | 1.72 | +5.5 |
| 9 | Fibroadenoma | 0.51 | 0.58 | +13.7 |
| 10 | Fibroadenoma | 1.42 | 1.41 | −0.7 |
| 11 | Fibroadenoma | 0.57 | 0.58 | +1.8 |
| 12 | Fibroadenoma | 0.41 | 0.59 | +43.9 |
| 13 | Fibroadenoma | 1.37 | 1.69 | +23.4 |
| 14 | Fibroadenoma | 0.37 | 0.51 | +37.8 |
| 15 | Invasive ductal carcinoma | 0.72 | 0.85 | +18.1 |
| 16 | Invasive ductal carcinoma | 1.03 | 0.96 | −6.8 |
| 17 | Invasive ductal carcinoma | 1.71 | 1.62 | −5.3 |
| 18 | Invasive ductal carcinoma | 1.77 | 1.64 | −7.3 |
| 19 | Invasive ductal carcinoma | 1.13 | 1.12 | −0.9 |
| 20 | Invasive ductal carcinoma | 1.52 | 1.84 | +21.1 |
| 21 | Invasive lobular carcinoma | 0.80 | 0.82 | +2.5 |
| 22 | Invasive lobular carcinoma | 1.37 | 1.69 | +23.4 |
| 23 | Intracystic papillary carcinoma | 0.51 | 0.52 | +2.0 |
| 24 | Adenocarcinoma | 1.02 | 0.98 | −3.9 |

RPM = reference phantom method. Column 5 gives the percentage difference between the attenuation coefficient estimated with the reference phantom method from that determined using the hybrid method.

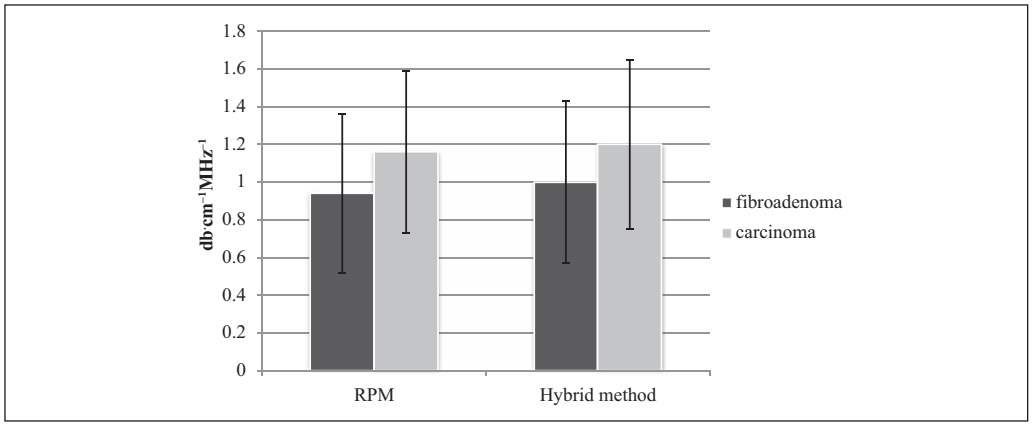


**Figure 1.** Average and standard deviation of the slopes of the attenuation coefficient versus frequency estimated using the RPM and hybrid method for fibroadenomas and carcinomas.
RPM = reference phantom method.

error bars indicate one standard deviation. The mean attenuation value of the carcinomas (1.16 $dB{\cdot}cm^{-1}MHz^{-1}$ and 1.20 $dB{\cdot}cm^{-1}MHz^{-1}$ for the RPM and the hybrid method, respectively) was somewhat greater than the mean attenuation value of the fibroadenomas (0.94 $dB{\cdot}cm^{-1}MHz^{-1}$ and 1.00 $dB{\cdot}cm^{-1}MHz^{-1}$ for the RPM and the hybrid method, respectively), and the standard deviation of these estimates for the two mass types are similar. The range of attenuation values for carcinomas overlaps the range of values found for fibroadenomas.

D'Astous and Foster[29] reported mean attenuation coefficient versus frequency slopes for five excised invasive ductal carcinomas as 0.86 $dB{\cdot}cm^{-1}MHz^{-1}$ at 7 MHz, while our results for six invasive ductal carcinomas were 1.32 $dB{\cdot}cm^{-1}MHz^{-1}$ and 1.33 $dB{\cdot}cm^{-1}MHz^{-1}$ from the RPM and hybrid method, respectively. In our study, the attenuation estimates were from in vivo breast masses, and the analyses used broader bandwidths.

## *Attenuation Coefficients and BI-RADS "Posterior Acoustic Features"*

In relating attenuation coefficients to "posterior acoustic features," the attenuation estimates from the RPM were chosen (since the estimates from the two methods were in agreement, so evidently, tissue inhomogeneities within the region of interest (ROI) did not compromise RPM determinations). Furthermore, in our experience, the RPM exhibits a lower variance for attenuation estimates in homogeneous phantoms.

The slopes of the attenuation coefficient versus frequency estimated using the RPM are listed again in Table 2 (column 4), along with each mass's stated posterior acoustic feature (column 3). The mean ± 1 standard deviation of the estimated attenuation coefficients was 0.75 ± 0.31 $dB{\cdot}cm^{-1}MHz^{-1}$ for masses that exhibited "enhancement"; values were 1.07 ± 0.38 $dB{\cdot}cm^{-1}MHz^{-1}$ for masses whose posterior acoustic features were said to be "none" and 1.56 ± 0.18 $dB{\cdot}cm^{-1}MHz^{-1}$ for masses judged to be "shadowing." Also presented in this table are the sonographer measured lesion dimensions (in the direction of beam propagation, column 5) as well as the products of the attenuation coefficient versus frequency slope and lesion diameter ("total attenuation," column 6).

The total attenuation estimate is plotted for each mass, along with its corresponding posterior acoustic feature in Figure 2. The mean ± 1 standard deviation of the estimated attenuation value times the lesion dimension along the acoustic beam was 0.70 ± 0.12 $dB{\cdot}MHz^{-1}$ for masses that exhibited "enhancement", 1.08 ± 0.44 $dB{\cdot}MHz^{-1}$ for masses whose posterior acoustic features were said to be "none" and 1.93 ± 0.76 $dB{\cdot}MHz^{-1}$ for masses judged to be "shadowing." As can be seen, there is potential to quantify parameters directly related to "posterior acoustic features." Relatively low values for the computed attenuation within the mass correspond to cases where echo enhancement was seen by the three readers; computed high attenuation values correspond to cases of "shadowing." QUS has an advantage of assessing the characteristics of the mass itself without subjective comparison with the surrounding tissues.

## *BSCs and BI-RADS "Echo Pattern"*

For each mass, BSCs were averaged over the 5-to-8-MHz range. The resultant "ABSC" for each mass is presented along with its corresponding echo pattern in Figure 3. No strong statements can be made about the utility of the echo pattern for lesion differentiation, nor of the degree of correlation of echo pattern findings with ABSC values, since nearly all tumors in this data set had "hypoechoic" findings. However, most tumors with ABSC values below 0.04 $cm^{-1}sr^{-1}$ were described as "hypoechoic." Another interesting finding is that most of the carcinomas exhibited very low ABSC.

The approximate mean BSC from five excised invasive ductal carcinomas measured by D'Astous and Foster[29] was 0.0008 $cm^{-1}sr^{-1}$ over 3 to 7 MHz. Our result for six in vivo invasive ductal carcinomas was 0.005 $cm^{-1}sr^{-1}$ over 5 to 8 MHz.

**Table 2.** Estimated Slopes of the Attenuation Coefficient versus Frequency Using the RPM, Lesion Dimensions along the Acoustic Beam, and Posterior Acoustic Feature Descriptors for 24 Breast Tumors.

| Patient Number | Biopsy Result | Posterior Acoustic Feature | RPM Result ($dB \cdot cm^{-1} MHz^{-1}$) | Lesion Dimension (cm) | Total Attenuation ($dB \cdot MHz^{-1}$) |
|---|---|---|---|---|---|
| 1 | Fibroadenoma | None | 1.06 | 0.9 | 0.954 |
| 2 | Fibroadenoma | Enhancement | 0.44 | 1.2 | 0.528 |
| 3 | Fibroadenoma | Combined | 0.97 | 1.4 | 1.358 |
| 4 | Fibroadenoma | None | 1.29 | 1.2 | 1.548 |
| 5 | Fibroadenoma | Enhancement | 1.12 | 0.8 | 0.896 |
| 6 | Fibroadenoma | Combined | 1.02 | 0.6 | 0.612 |
| 7 | Fibroadenoma | Enhancement | 1.01 | 0.7 | 0.707 |
| 8 | Fibroadenoma | None | 1.63 | 0.8 | 1.304 |
| 9 | Fibroadenoma | Enhancement | 0.51 | 1.2 | 0.612 |
| 10 | Fibroadenoma | Shadowing | 1.42 | 1.7 | 2.414 |
| 11 | Fibroadenoma | None | 0.57 | 0.7 | 0.399 |
| 12 | Fibroadenoma | Enhancement | 0.41 | 1.4 | 0.574 |
| 13 | Fibroadenoma | Combined | 1.37 | 0.8 | 1.096 |
| 14 | Fibroadenoma | Combined | 0.37 | 1.2 | 0.444 |
| 15 | Invasive ductal carcinoma | None | 0.72 | 1.1 | 0.792 |
| 16 | Invasive ductal carcinoma | Enhancement | 1.03 | 0.8 | 0.824 |
| 17 | Invasive ductal carcinoma | Shadowing | 1.71 | 1.4 | 2.394 |
| 18 | Invasive ductal carcinoma | Shadowing | 1.77 | 0.5 | 0.885 |
| 19 | Invasive ductal carcinoma | None | 1.13 | 1.3 | 1.469 |
| 20 | Invasive ductal carcinoma | Shadowing | 1.52 | 1.7 | 2.584 |
| 21 | Invasive lobular carcinoma | Combined | 0.80 | 1.8 | 1.44 |
| 22 | Invasive lobular carcinoma | Shadowing | 1.37 | 1.0 | 1.37 |
| 23 | Intracystic papillary carcinoma | Enhancement | 0.51 | 1.4 | 0.714 |
| 24 | Adenocarcinoma | Enhancement | 1.02 | 0.7 | 0.714 |

RPM = reference phantom method. Total attenuation was calculated as a product of the slope of the attenuation coefficient versus frequency and lesion dimension.

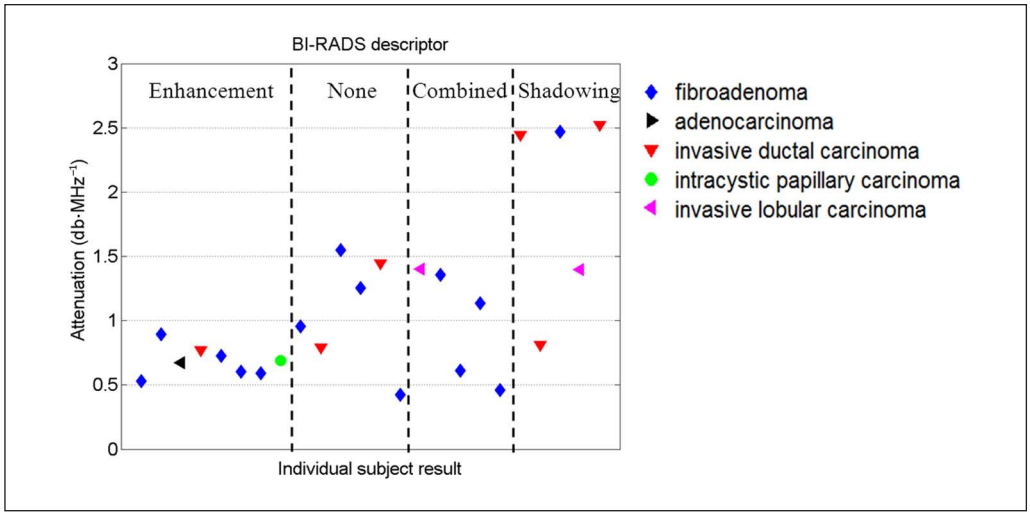


**Figure 2.** Total attenuation (product of the slope of the attenuation coefficient vs. frequency and lesion dimension) in each mass, categorized according to its BI-RADS descriptor, "posterior acoustic features."

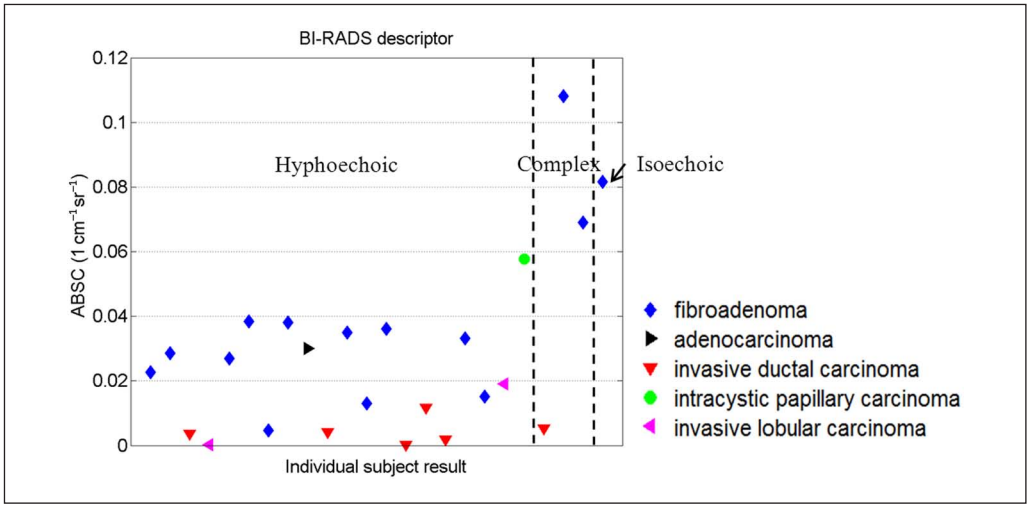


**Figure 3.** Averaged BSC for each mass, categorized according to its BI-RADS "echo pattern."

### *ABSCs versus Attenuation Coefficient*

We also investigated whether combining attenuation and backscatter results might improve the ability to differentiate malignant from benign masses. The ABSCs versus attenuation coefficients (slope of attenuation coefficient vs. frequency) are plotted in Figure 4. This is analogous to the plots by D'Astous and Foster[29] although their work involved excised tissue.

### *ESD Estimation*

The estimated ESDs over the ROI were averaged for each breast mass. The mean and "heterogeneity index" (HI) of the ESD values are presented in Figure 5. A HI here is defined as a square root of the ESD variances (ignoring parameter estimate correlations from overlapping regions) within the PER. Although the mean ESD alone did not differentiate the mass type, most of the fibroadenomas had more variation in ESD within the ROI than did carcinomas in this study.

## Discussion

The intent of the work reported here was to determine whether quantitative measures of attenuation and backscatter were consistent with subjectively assessed BI-RADS parameters that describe these phenomena. The hypothesis was that quantitative assessments of these parameters add more information by conveying information, such as "How much does it shadow?" and "How hypoechoic is it?" Since these parameters are assessed computationally, there is great potential for them to be assessed automatically in a computer-aided diagnosis algorithm.

Estimates of ultrasound attenuation within breast masses done using a RPM and a hybrid frequency shift technique were in agreement, except for two fibroadenoma cases. In one of these, Patient 12 in Table 2, there is evidence of specular reflection within the ROI as seen in Figure 6a. Backscatter changes affect the RPM to a much greater degree than they do the hybrid method, and this likely is the reason for this discrepancy.[49] The accuracy of RPM attenuation estimates might be improved if methods to account for these backscatter changes were available. One approach that holds promise is to test for the presence of a significant coherent component

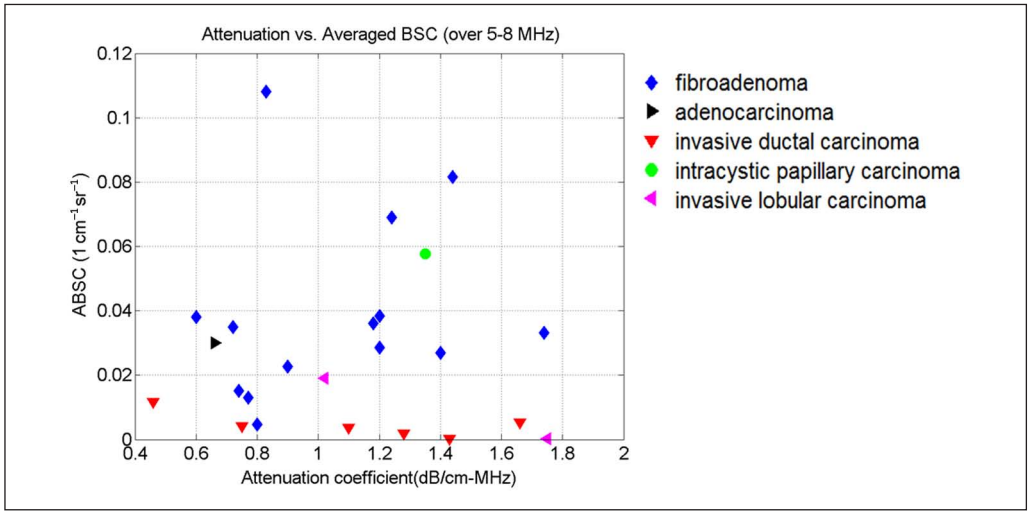


**Figure 4.** Averaged BSC versus attenuation coefficient (slope of attenuation coefficient vs. frequency) for individual masses.

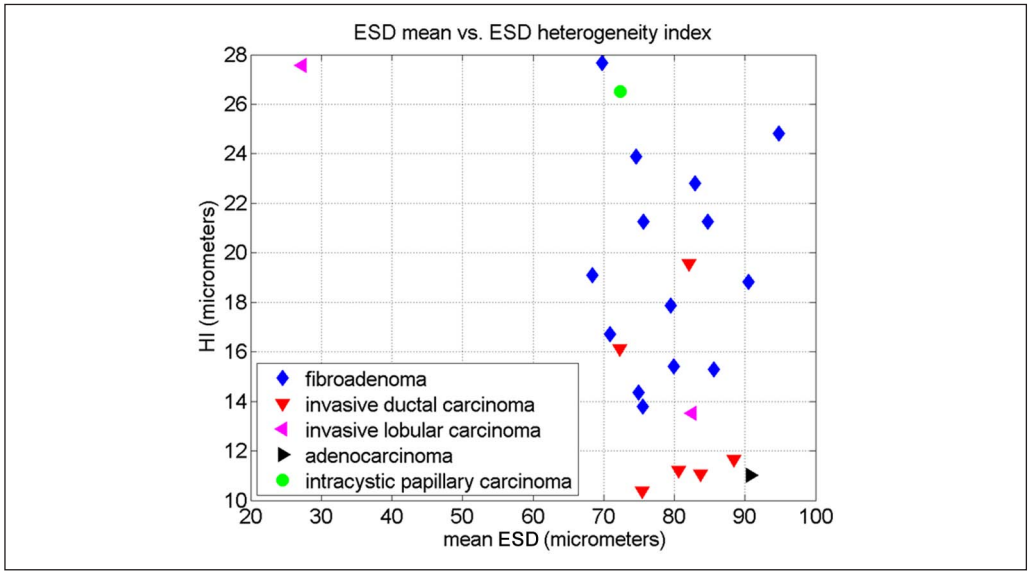


**Figure 5.** ESDs (calculated from 5 to 8 MHz) over the ROI were averaged, and the mean and heterogeneity index are plotted for each mass.
HI = heterogeneity index; ESD = effective scatterer diameters.

in the echo signals[50] and use that information to avoid ROIs that violate the assumption of incoherent scattering.[49] This will be a topic for future studies.

Another case where disagreement exists between values obtained with the two attenuation estimation methods is Patient 14 (Figure 6b). Here, a B-mode image of the mass exhibits a "complex" echo pattern. Such a feature would be difficult to characterize by a single BSC or a

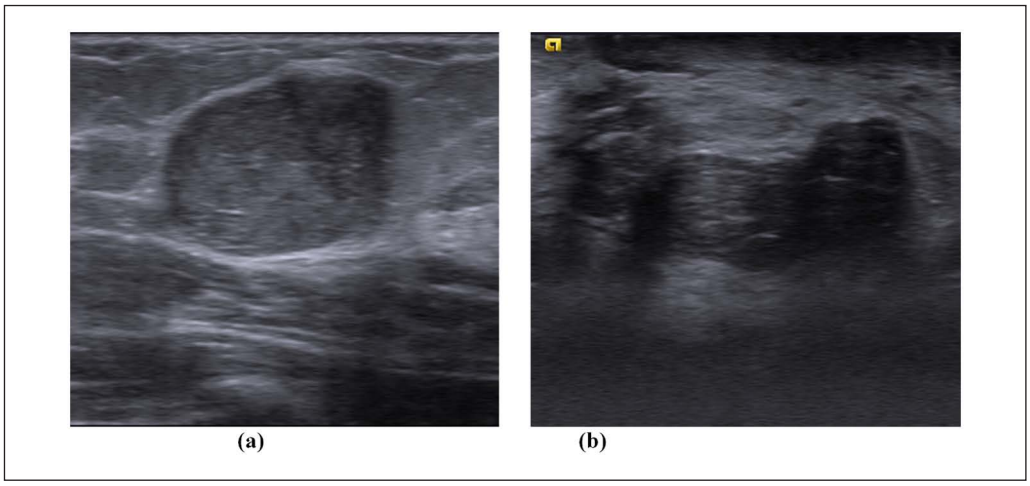


**Figure 6.** B-mode images of a breast mass: (a) Patient 12, (b) Patient 14.

single attenuation coefficient. Note, however, in the present study, the QUS representation for each mass was simplified because the study was focused on relating BI-RADS descriptors to attenuation and backscattering. It may prove useful to generate attenuation and ABSC maps within an ROI to more thoroughly describe spatial variations within breast masses.

Nevertheless, the consistency between attenuation estimates using the hybrid method and the RPM is encouraging. The results motivate continued investigation into quantitative in vivo breast mass attenuation estimation since, at the moment, there is little published data on quantitative acoustical properties, including the degree of variability among specific types of masses.

In general, there was good correspondence between posterior acoustic features and measured attenuation for each mass. There were some masses, however, that did not follow the expected trend. A "total attenuation" for each mass was calculated by multiplying the attenuation coefficient by the lesion dimension along the acoustic scan line. As pointed out above, breast masses (especially ones with "complex" echo patterns or "combined" posterior acoustic feature) likely possess complexity that a single attenuation estimate would not capture. We believe further refinement in attenuation estimations, including computing attenuation coefficient maps, is worth pursuing to continue to study this property.

The BI-RADS-expressed "echo patterns" within masses agreed well with the ABSC values. Since all but three masses in the study were judged to be "hypoechoic," more data will be needed to draw conclusions regarding this preliminary result. In Figure 3, most carcinomas had relatively low ABSCs suggesting that quantitative backscatter levels could also provide additional diagnostic information. For example, the study by Hong et al.[13] showed that among 403 masses, those judged "isoechoic" and "hypoechoic" had 12% prevalence and 80% prevalence, respectively. Thus, most breast masses viewed on clinical ultrasound scans are characterized with one of these two descriptions, so it is hard to classify masses based on echo patterns. On the other hand, there is no gradation within the term *hypoechoic* (How hypoechoic is it?), and the results in Figure 3 suggest that characterizing tumors with an absolute quantity might improve differentiation. Although some cancers have relatively high ABSC values, most exhibit low values compared with ABSCs from benign tumors. ABSC and attenuation values were evaluated together for differentiating fibroadenomas from carcinomas, and demonstrated modest performance.

The ESD was calculated to assess the variability of the frequency dependence of BSCs among masses. As seen in Figure 5, the mean and HI of ESD estimates fell into a narrow range of values for our patient data. However, the ESD and HI pair could be combined to separate most fibroadenomas from carcinomas. It should be noted that the bandwidth used for ESD estimation (5-8 MHz) was quite narrow, and thus the estimated ESD likely have relatively high uncertainty. Relatively broadband data are needed for accurate ESD estimations.[51] In the future, the comparison of ESD estimates using all available bandwidths should be tested. A more robust differentiator would likely include these and other features, such as the mass shape, margin, and orientation that could be quantized and used with other factors, such as patient demographics for improved risk stratification.

One limitation to this study was a possible sound speed mismatch between reference phantoms and tissues during data collection. The sound speed of the reference phantom was 1490 m/s. To minimize any effects related to a mismatch in the speed of sound we have begun collecting data with the transducer transmit focus set distal to the lesion being scanned. Nam et al.[52] found this the most optimal configuration for reducing errors in the estimated attenuation coefficient. However, further effort to match all sound speeds will be needed in the future to reduce any possible error in estimation of QUS parameters.

## Conclusion

Except for two complex masses, attenuation coefficients of breast tumors estimated using the RPM were consistent with those estimated using a hybrid method. This demonstrates the potential for quantitative attenuation estimates in breasts. The product of the slope of the attenuation coefficient versus frequency, and the lesion dimension was used to compute the total attenuation in breast masses. That value correlated with the subjectively assessed "posterior acoustic feature" and has potential as a quantitative measure to supplement that BI-RADS descriptor. ABSC values correlated with the subjectively determined "echogenicity" within breast masses. The combination of ABSC and attenuation coefficient showed limited utility in differentiating fibroadenomas and carcinomas. Finally, most fibroadenomas exhibited relatively high variation in ESD estimates within the mass compared with that of carcinomas.

## Acknowledgment

We are grateful for the assistance by Dr. Gale Sisney who performed the breast imaging–reporting and data system assessment.

## Declaration of Conflicting Interests

The author(s) declared no potential conflicts of interest with respect to the research, authorship, and/or publication of this article.

## Funding

The author(s) disclosed receipt of the following financial support for the research, authorship, and/or publication of this article: This work was supported by the National Institutes of Health Grant R01CA111289.

## References

1. Mandelson MR, Oestreicher N, Porter PL, White D, Finder CA, Taplin SH, et al. Breast density as a predictor of mammographic detection: comparison of interval- and screen-detected cancers. J Natl Cancer Inst. 2000;92:1081-87.

2. Jackson VP, Reynolds HE, Hawes DR. Sonography of the breast. Semin Ultrasound CR MR. 1996;17:460-75.
3. Stavros AT, Thinkman D, Rapp CL, Dennis MA, Parker SH, Sisney GA. Solid breast nodules: use of sonography to distinguish between benign and malignant lesions. Radiology. 1995;196:123-34.
4. Jackson VP. Management of solid breast nodules: what is the role of sonography? Radiology. 1995;196:14-15.
5. Paulinelli RR, Freitas-Junior R, Moreira MA, de Moraes VA, Bernardes-Junior JR, Vidal Cda S, et al. Risk of malignancy in solid breast nodules according to their sonographic features. J Ultrasound Med. 2005;24:635-41.
6. Paulinelli RR, Freitas-Junior R, de Lucena CÊ, Moreira MA, de Moraes VA, Bernardes-Junior JR, Vidal Cda S, et al. Sonobreast: prediction individualized probabilities of malignancy in solid breast masses with echographic expression. Breast J. 2011;17:152-59.
7. Stavros AT. Breast Ultrasound. Philadelphia, PA: Williams and Mosby; 1996.
8. Helmut M. The Practice of Breast Ultrasound: Techniques, Findings, Differential Diagnosis. New York: Thieme; 2000.
9. Sehgal CM, Weinstein SP, Arger PH, Conant EF. A review of breast ultrasound. J Mammary Gland Biol Neoplasia. 2006;11:113-23.
10. Arger PH, Sehgal CM, Conant EF, Zuckerman J, Rowling SE, Patton JA. Interreader variability and predictive value of US descriptions of solid breast masses: pilot study. Acad Radiol. 2001;8:335-42.
11. Rahbar G, Sie AC, Hansen GC, Prince JS, Melany ML, Reynolds HE, et al. Benign versus malignant solid breast masses: US differentiation. Radiology. 1999;213:889-94.
12. American College of Radiology. BI-RADS: ultrasound. 1st ed. In: Breast Imaging Reporting and Data System: BI-RADS Atlas. 4th ed. Reston, VA: American College of Radiology; 2003.
13. Hong AS, Rosen EL, Soo MS, Baker JA. BI-RADS for sonography: positive and negative predictive values of sonographic features. Am J Roentgenol. 2005;184:1260-65.
14. Liberman L, Abramson AF, Squires FB, Glassman JR, Morris EA, David Dershaw D. The breast imaging reporting and data system: positive predictive value of mammographic features and final assessment categories. Am J Roentgenol. 1998;171:35-40.
15. Fujii Y, Taniguchi N, Itoh K, Shigeta K, Wang Y, Tsao JW, et al. A new method for attenuation coefficient measurement in the liver: comparison with the spectral shift central frequency method. J Ultrasound Med. 2002;21:783-88.
16. Narayana PA, Ophir J. On the frequency dependence of attenuation in normal and fatty liver. IEEE Trans Ultrason. 1983;30:379-83.
17. Wear KA. Characterization of trabecular bone using the backscattered spectral centroid shift. IEEE Trans Ultrason Ferroelectr Freq Control. 2003;50:402-407.
18. Sasso M, Haïat G, Yamato Y, Naili S, Matsukawa M. Dependence of ultrasonic attenuation on bone mass and microstructure in bovine cortical bone. J Biomech. 2008;41:347-55.
19. Golub RM, Parsons RE, Sigel B, Feleppa EJ, Justin J, Zaren HA, et al. Differentiation of breast tumors by ultrasonic tissue characterization. J Ultrasound Med. 1993;12:601-608.
20. Huang SW, Li PC. Ultrasonic computed tomography reconstruction of the attenuation coefficient using a linear array. IEEE Trans Ultrason Ferroelectr Freq Control. 2005;52:2011-22.
21. Liu T, Lizzi FL, Silverman RH, Kutcher GJ. Ultrasonic tissue characterization using 2-D spectrum analysis and its application in ocular tumor diagnosis. Med Phys. 2004;31:1032-39.
22. Feleppa EJ, Machi J, Noritomi T, Tateishi T, Oishi R, Yanagihara E, et al. Differentiation of metastatic from benign lymph nodes by spectrum analysis in vitro. Proc IEEE Ultrason Symp. 1997;2:1137-42.
23. Mamou J, Coron A, Hata M, Machi J, Yanagihara E, Laugier P, et al. Three-dimensional high-frequency characterization of cancerous human lymph nodes. Ultrasound Med Biol. 2010;36:361-75.
24. Feleppa EJ, Urban S, Kalisz A, Lizzi FL, Fair WR, Porter CR. Advanced ultrasonic imaging of the prostate for guiding biopsies and for planning and monitoring therapy. Proc IEEE Ultrason Symp. 2000;2:1399-403.

25. Insana MF, Hall TJ, Wood JG, Yan ZY. Renal ultrasound using parametric imaging techniques to detect changes in microstructure and function. Invest Radiol. 1993;28:720-25.
26. Wilson T, Chen Q, Zagzebski JA, Varghese T, VanMiddlesworth L. Initial clinical experience imaging scatterer size and strain in thyroid nodules. J Ultrasound Med. 2006;25:1021-29.
27. Liu W, Zagzebski JA, Kliewer MA, Varghese T, Hall TJ. Ultrasonic scatterer size estimations in liver tumor differentiation. Med Phys. 2007;34:2597.
28. Oelze ML, O'Brien WD Jr, Blue JP, Zachary JF. Differentiation and characterization of rat mammary fibroadenomas and 4T1 mouse carcinomas using quantitative ultrasound imaging. IEEE Trans Med Imaging. 2004; 23:764-71.
29. D'astous FT, Foster FS. Frequency dependence of ultrasound attenuation and backscatter in breast tissue. Ultrasound Med Biol. 1986;12:795-808.
30. Brunke SS, Insana MF, Dahl JJ, Hansen C, Ashfaq M, Ermert H. An ultrasound research interface for a clinical system. IEEE Trans Ultrason Ferroelectr Freq Control. 2007;54:198-210.
31. Wear KA, Stiles TA, Frank GR, Madsen EL, Cheng F, Feleppa EJ, et al. Inter-laboratory comparison of ultrasonic backscatter coefficient measurements from 2 to 9 MHz. J Ultrasound Med. 2005;24:1235-50.
32. Chen JF, Zagzebski JA, Madsen EL. Tests of backscatter coefficient measurement using broadband pulses. IEEE Trans Ultrason Ferroelectr Freq Control. 1993;40:603-607.
33. Rosado-Mendez IM, Nam K, Hall TJ, Zagzebki JA. Performance of various spectral estimation methods on acoustic backscatter coefficient estimation under data size limitations. In: Institute of Electrical and Electronics Engineers ( IEEE ) Xplore Digital Library Ultrasonics Symposium Proceedings, Orlando, FL, 18-21 October; 2011, pp 49-52
34. Hall TJ, Zhu Y, Spalding CS. In vivo real-time freehand palpation imaging. Ultrasound Med Biol. 2003;29:427-35.
35. Madsen EL, Hobson MA, Shi H, Varghese T, Frank GR. Stability of heterogeneous elastography phantoms made from oil dispersions in aqueous gels. Ultrasound Med Biol. 2006;32:261-70.
36. Yao LX, Zagzebski JA, Madsen EL. Backscatter coefficient measurements using a reference phantom to extract depth-dependent instrumentation factors. Ultrason Imaging. 1990;2:58-70.
37. Kim H, Varghese T. Hybrid spectral domain method for attenuation slope estimation. Ultrasound Med Biol. 2008;34:1808-19.
38. Nam K, Zagzebski JA, Hall TJ. Simultaneous backscatter and attenuation estimation using a least squares method with constraints. Ultrasound Med Biol. 2011;37:2096-104.
39. Welch PD. The use of fast Fourier transforms for the estimation of power spectra: a method based on time averaging over short modified periodograms. IEEE Trans Audio Electroacoust. 1967;15:70-73.
40. Rabiber L, Schafer R, Rader C. The chirp z-transform algorithm. IEEE Trans Audio Electroacoust. 1969;17:86-92.
41. Hall TJ, Insana MF, Harrison LA, Cox GG. Ultrasonic measurement of glomerular diameters in normal adult humans. Ultrasound Med Biol. 1996;22:987-97.
42. Roberjot V, Laugier P, Droin P, Giat P, Berger G. Measurement of intergrated backscatter coefficient of trabecular bone. Proc IEEE Ultrason Symp. 1996;2:1123-26.
43. Kuc R, Schwartz M. Estimating the acoustic attenuation coefficient slope for liver from reflected ultrasound signals. IEEE Trans Sonics Ultrason. 1979;26:353-62.
44. Nassiri DK, Hill CR. The use of angular scattering measurements to estimate structural parameters of human and animal tissues. J Acoust Soc Am. 1986;79:2048-54.
45. Nicholas D. Evaluation of backscattering coefficients for excised human tissues: results, interpretation, and associated measurements. Ultrasound Med Biol. 1982;8:17-28.
46. Bamber JC. Theoretical modeling of the acoustic scattering structure of human liver. Acoust Lett. 1979;3:114-19.
47. Insana MF, Wagner RF, Brown DG, Hall TJ. Describing small-scale structure in random media using pulse-echo ultrasound. J Acoust Soc Am. 1990;87:179-92.

48. Oelze ML, O'Brien WD Jr. Method of improved scatter size estimation and application to parametric imaging using ultrasound. J Acoust Soc Am. 2002;112:3053-63.
49. Luchies AC WD, Ghoshal G, O'Brien WD Jr, Oelze ML. Quantitative ultrasonic characterization of diffuse scatterers in the presence of structures that produce coherent echoes. IEEE Trans Ultrason Ferroelectr Freq Control. 2012;59:893-904.
50. Donohue KD, Huang L, Burks T, Forsberg F, Piccoli CW. Tissue classification with generalized spectrum parameters. Ultrasound Med Biol. 2001;27:1505-14.
51. Insana MF, Hall TJ. Parametric ultrasound imaging from backscatter coefficient measurements: image formation and interpretation. Ultrasonic Imaging. 1990;12:245-67.
52. Nam K, Rosado-Mendez IM, Rupert NC, Madsen EL, Zagzebski JA, Hall TJ. Effects of sound speed mismatch on ultrasound attenuation measurements using reference phantoms. Ultrasonic Imaging. 2011;33:251-63.